J Mater Sci: Mater Electron (2015) 26:353–359
DOI 10.1007/s10854-014-2407-z

Facile synthesis of α-MnO_2 nanowires/spherical activated carbon composite for supercapacitor application in aqueous neutral electrolyte

Zesheng Li · Zhenghui Liu · Dehao Li · Bolin Li · Qingyu Li · Youguo Huang · Hongqiang Wang

Received: 10 September 2014 / Accepted: 17 October 2014 / Published online: 6 December 2014

Abstract One-dimensional (1-D) α-MnO_2 nanowires/spherical activated carbon composite, namely the α-MnO_2 nanowires growth onto the surface of activated mesocarbon microbeads (a-MCMB), has been prepared by using a simple hydrothermal synthesis method. The α-MnO_2 nanowires are found to be less than 50 nm in diameter and have a characteristic length up to 2 μm. The novel α-MnO_2 nanowires/a-MCMB composite when used for supercapacitor electrode material exhibits a specific capacitance (C_s) of 357 F g^{-1} in 1 M Na_2SO_4 aqueous neutral solution. The C_s based on the α-MnO_2 nanowires is estimated to be as high as 890 F g^{-1}. A good cycling stability of this composite material is also demonstrated for supercapacitor application.

1 Introduction

Electrochemical capacitor or supercapacitor is a type of burgeoning energy-storage electronic devices, behaving electronic features between conventional dielectric capacitors and batteries [1–3]. Supercapacitor can be categorized as two types: electrical double-layer capacitor with activated carbon materials as electrodes [4], and Faradic pseudo-supercapacitors with metal oxides as electrodes [5]. Manganese dioxide (MnO_2) has been considered to be one promising electrode materials for pseudo-supercapacitors due to its excellent electrochemical performances, abundant resources and environmental compatibility [6, 7]. Recently, a variety of one-dimensional (1-D) MnO_2 nanostructures, including nanowires, nanorods, nanotubes and nanofibers have received great research attention due to their unique nanostructures [8, 9].

The development of 1-D MnO_2 nanostructures offers significant opportunities to improve the performances of pseudo-supercapacitors because these 1-D nanostructures not only have sufficiently high surface area, but also have the smallest dimension with high aspect ratio compared with those of bulky or nanoparticle structures, which will provide a shorter cation diffusion path for supercapacitor application [10]. However, the pure MnO_2 nanomaterials were usually faced with the problem of low electric conductivity and poor stability [11, 12], which limit their maximal capacitance and long-term application for supercapacitors. Therefore, it is of great significance to develop a facile and effective strategy to enhance capacitive performance of 1-D MnO_2 nanomaterials.

To date, in situ growth of carbon-supported MnO_2 nanostructures is greatly attractive and the resulting MnO_2/C composite has already been widely applied as electrode materials for supercapacitors which can provide both high capacitance and good cycle life [13–15]. It was known that mesocarbon microbead (MCMB) can be used to fabricate spherical activated carbon (activated mesocarbon microbead, a-MCMB) with high surface area (nearly 3,000 m^2 g^{-1}) by chemical activation with KOH [16, 17], which is extremely desirable for the formation of

Z. Li (✉) · Z. Liu · D. Li · B. Li
Development Center of Technology for Petrochemical Pollution Control and Cleaner Production of Guangdong Universitites, College of Chemical Engineering, Guangdong University of Petrochemical Technology, Maoming 525000, Guangdong, China
e-mail: lzs212@163.com

Q. Li · Y. Huang · H. Wang (✉)
Key Laboratory for the Chemistry and Molecular Engineering of Medicinal Resources (Ministry of Education of China), School of Chemistry and Chemical Engineering of Guangxi Normal University, Guilin 541004, Guangxi, China
e-mail: hqw74@163.com

electric double layer capacitance by ion adsorption of electrolyte on the pore surface. The high-surface-area spherical activated carbon is expected to be one of promising carbon supports for the preparation of high-performance MnO_2/C composite electrode for supercapacitors.

It is well known that MnO_2 has several crystallographic forms, including α, β, γ, δ and λ forms, in which the α, β and γ forms has 1-D tunnel structures, δ form has a 2-D layered structures and λ form has 3-D spinel structures [18]. Because the capacitance properties largely depend on the intercalation/deintercalation level of protons or cations into MnO_2 matrix, some crystallographic forms, such as 1-D tunnel structures, with sufficient accommodated gaps for the ions, are particularly expected to be of high capacitance [19]. Consequently, the α-MnO_2 is widely considered to be one of candidate electrodes for high-performance supercapacitor due to its advantaged crystallographic structure and really accessible nanostructures [20–22].

In this study, using the high-surface-area a-MCMB as the substrate, we develop an efficient hydrothermal procedure for the preparation of α-MnO_2 nanowires/a-MCMB composite electrode. To our knowledge, it is the first time to design 1-D α-MnO_2 nanostructures onto spherical activated carbon for the application in energy-storage electronic devices. The electrochemical properties of this novel α-MnO_2 nanowires/a-MCMB composite have been investigated as high-performance electrode material for supercapacitors in 1 M Na_2SO_4 aqueous neutral solution.

2 Experimental

The raw MCMB with a specific surface area of 32.6 m^2 g^{-1} was supplied by Tianjin Tiecheng battery Co. Ltd., China. In order to improve the specific surface area, the initial MCMB was chemically activated by KOH as follows: the MCMB was mixed with KOH (5:1, w/w) in deionized water to obtain a homogeneous slurry, and then the slurry was heated at a rate of 2 °C min^{-1} up to 850 °C and was held for 1 h at that temperature in Ar flow in a tubular furnace. Finally, the a-MCMB was obtained by washing with 5 wt%. HCl solution and deionized water. A hydrothermal synthesis method was applied to prepare MnO_2/a-MCMB composite: typically, 0.5 g a-MCMB, 0.49 g $KClO_3$ and 0.32 g $MnSO_3$ were dispersed in 25 mL deionized water and 15 mL concentrated HNO_3, and sonicated for about 15 min in an ultrasonic bath. Afterwards, the mixture was ransferred into a Teflon-lined stainless steel autoclave with 50 mL capacity, the autoclave was sealed and maintained at 120 °C for 12 h. After being allowed to cool to room temperature naturally, the MnO_2/a-MCMB product was centrifuged and washed repeatedly with distilled water to remove the excess reactants.

The specific surface areas of the samples were investigated by measuring nitrogen adsorption isotherm at 77 K on an automatic volumetric sorption analyzer. X-ray diffraction (XRD) patterns of the samples were determined using a diffractometer with Cu-K α1 radiation (λ = 0.15406 nm). The surface morphologies of the samples were observed using a field-emission scanning electron microscope (FE-SEM) and transmission electron microscope (TEM). In addition, inductively coupled plasma-atomic emission spectrometry (ICP-AES) was also used to analyze MnO_2 content in the composite using the method reported in the literature: the MnO_2/a-MCMB composite was first digested into 10 % HNO_3 solution at boiling temperature, and then the soluble Mn^{2+} in the solution was measured by ICP-AES.

Both MnO_2/a-MCMB composite and a-MCMB were prepared into electrodes (denoted as MnO_2/a-MCMB composite electrode and pristine a-MCMB electrode) and assembled into capacitor cells (1 M Na_2SO_4 aqueous solution as electrolyte) as follows: Firstly, the active substance was mixed with acetylene black and polytetrafluoroethylene (90:5:5, w/w/w) in ethanol to form a sticky slurry, then the slurry was rolled into a film (80–100 μm in thickness) before cut into disk electrodes with diameter of 10 mm. Subsequently, supercapacitor cells (two-electrode system) were assembled with a pair of electrodes and a piece of microporous separator between them. The cyclic voltammetry (CV) and electrochemical impedance spectroscopy (EIS) was recorded on an electrochemical workstation (ZAHNER IM6, Germany). For the sake of accuracy, the C_s of the electrode was obtained by using the two-electrode cell on a battery tester (Neware, Shenzhen, China).

3 Results and discussions

XRD patterns of as-prepared a-MCMB and MnO_2/a-MCMB composite samples are shown in Fig. 1. For the a-MCMB, the two weak peaks at 2θ ≈ 24° and 43°, corresponding to the (002) (marked in filled circle) and (101) diffraction peaks (marked in inverted triangle) of carbon, are very broad and weak, which suggests that the a-MCMB have a typical amorphous structure of activated carbon. For the MnO_2/a-MCMB, the sharp and clear diffraction peaks clearly indicate that the as-prepared MnO_2 has a good crystallinity. All the reflections of the MnO_2 can be indexed to a pure tetragonal phase [space group: I4/m (No. 87)] of a-MnO_2 (JCPDS 44-0141). In addition, a wide peak at 2θ ≈ 24.8° of a-MCMB (marked in filled circle) could be observed for MnO_2/a-MCMB, which suggests the composite structure based on MnO_2 and a-MCMB has been achieved via the simple hydrothermal synthesis method.

Typical SEM images of MnO_2/a-MCMB composite were presented in Fig. 2a, b. Figure 2a is a panoramic view

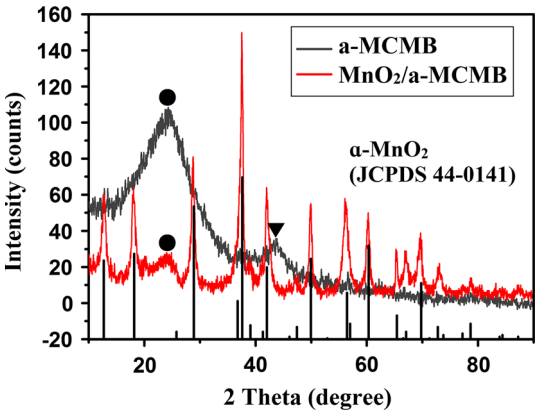

Fig. 1 XRD patterns of pristine a-MCMB and MnO_2/a-MCMB composite

of the composite sphere that depicts a good coverage of fibre-like MnO_2 on the surface of a-MCMB. And obvious 1-D nanostructures of MnO_2 nanowires (<50 nm in diameter and up to 2.0 μm in length) can be observed from the higher magnification images in Fig. 2b. Particularly, these MnO_2 nanowires display a good porous network framework, which indicates that the self-assembly growth of MnO_2 nanowires onto the a-MCMB has occurred in the hydrothermal condition. Figure 2c describes the SEM–EDS elemental mapping images of C, O and Mn from the MnO_2/a-MCMB composite. It is obvious that the C, O and Mn elements are homogeneously distributed corresponding to the selected SEM image. In addition, the TEM images as shown in Fig. 3 also demonstrate the well 1-D nanostructures of these MnO_2 nanowires with diameter from 10 to 40 nm.

Nitrogen adsorption–desorption isotherms of pristine a-MCMB and MnO_2/a-MCMB composite are shown in Fig. 4. The present isotherms exhibits the typical characteristics of mesoporous materials, with increasing adsorption volume as well as pronounced desorption hysteresis loops. The specific surface area (S_{BET}) of a-MCMB and MnO_2/a-MCMB composite, calculated by the Brunauer–Emmett–Teller (BET) equation are 2,890 and 2,512 $m^2\ g^{-1}$, respectively. The content of MnO_2 in the total composite is 15.62 wt% determined by ICP-AES analysis. The higher density of MnO_2 than the activated carbon may account for the loss in

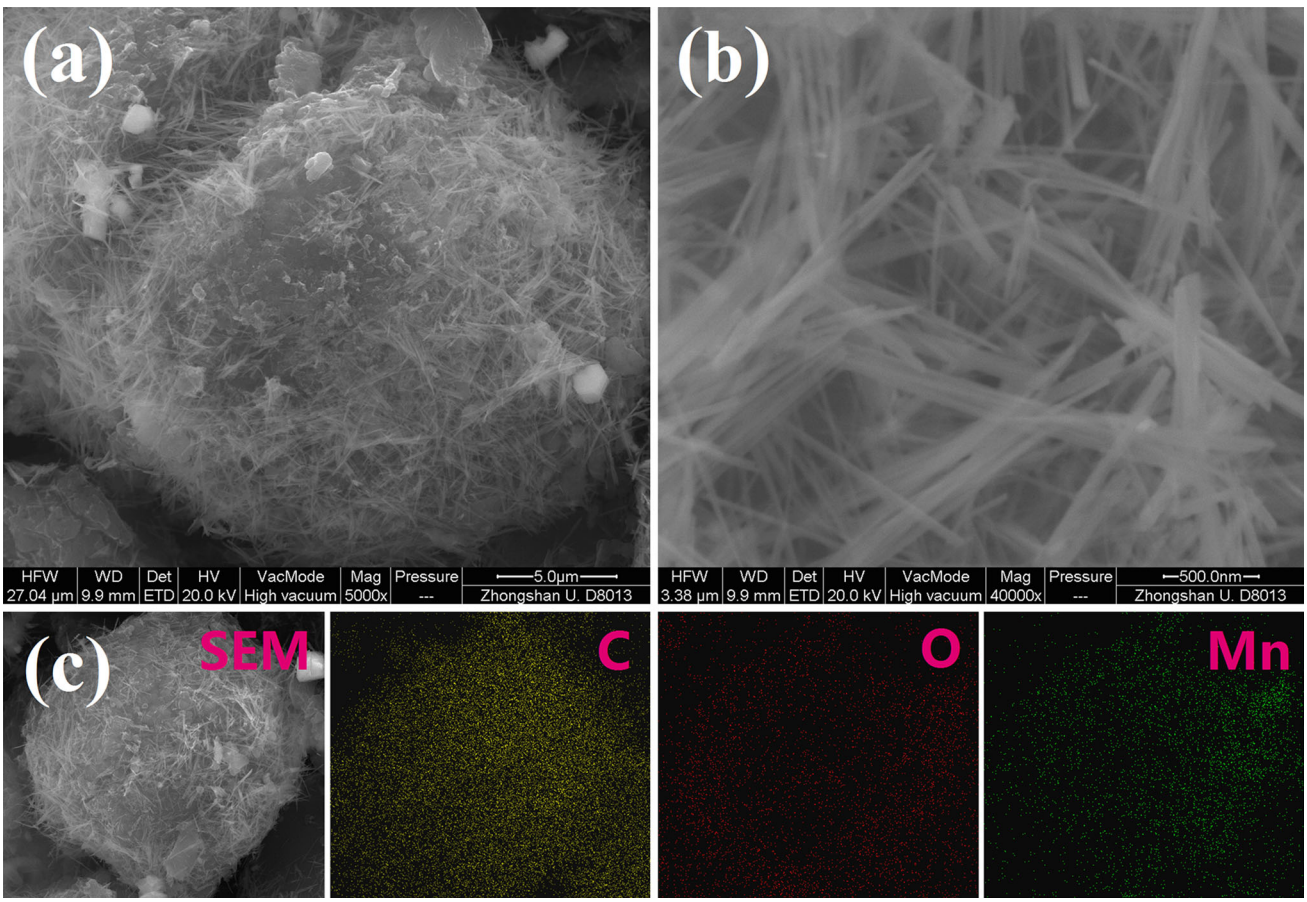

Fig. 2 SEM images **a**, **b** and SEM–EDS mapping images, **c** of MnO_2/a-MCMB composite

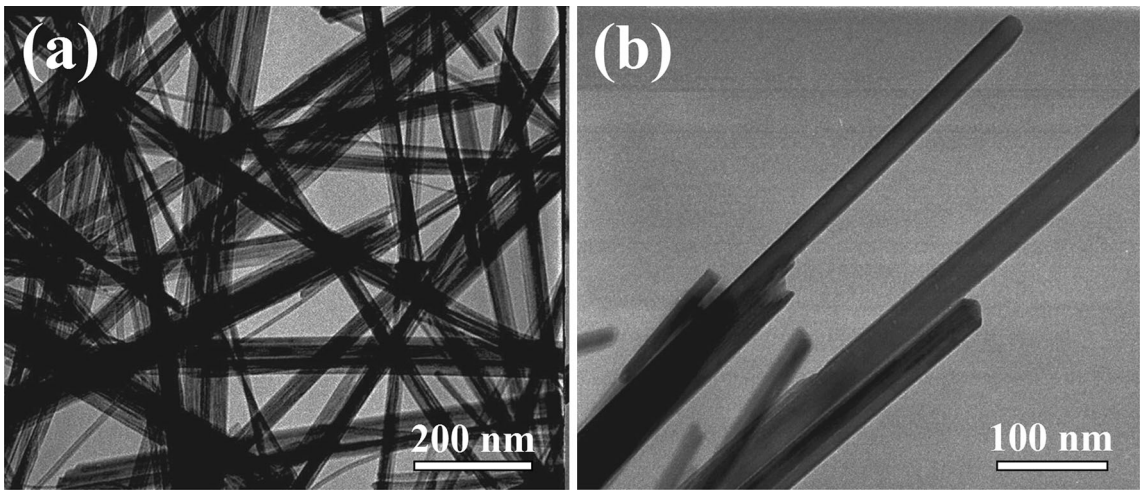

Fig. 3 TEM images of MnO_2 nanorods at different magnification images

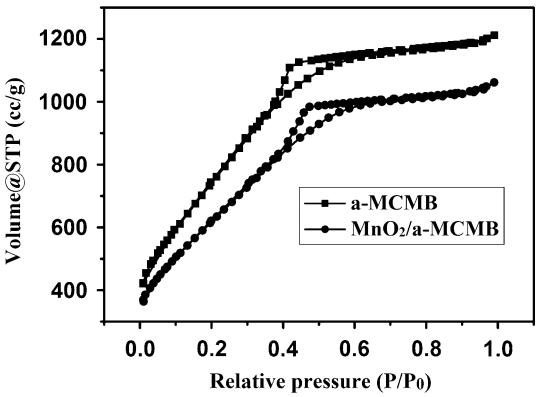

Fig. 4 Nitrogen adsorption–desorption isotherms of pristine a-MCMB and MnO_2/a-MCMB composite

Fig. 5 Pictures of the as-assembled supercapacitors: disk electrodes pressed on the stainless steel current collectors (*left*) and coin-type two-electrode cells (*right*)

S_{BET} of composite. It can be deduced that, compared with the traditional deposited distribution of MnO_2 nanoparticles, the porous network framework of MnO_2 nanowires enveloped on the a-MCMB may cause less influence to the porous structure of activated carbon. So it is believed that the high specific surface area of MnO_2/a-MCMB will help to improve utilization of composite material, and thus results in desirable capacitance in supercapacitor applications.

The capacitance performances of the as-prepared electrodes were investigated in 1 M Na_2SO_4 aqueous solution by assembling two-electrode supercapacitor cells. The pictures of as-assembled supercapacitors are shown in Fig. 5, which typically consists of two electrodes (disk electrodes pressed on current collectors). The CV curves of the MnO_2/a-MCMB composite electrode and pristine a-MCMB electrode in supercapacitor cells at scan rate of 10 mV s^{-1} are depicted in Fig. 6. It is obvious that, at potential region of 0.0–1.0 V, the curves of both the pristine a-MCMB electrode and the MnO_2/a-MCMB composite electrode have good rectangular shapes, which indicates good capacitive performances of the supercapacitors. Figure 6 also demonstrates that the CV area of the composite electrode is bigger than that of the pristine a-MCMB electrode, which indicates the improvement in capacitance of the composite electrode due to the redox-reaction of metal oxide.

Figure 7 presents the CV curves of the MnO_2/a-MCMB composite electrode in supercapacitor cells at different rates (10, 40 and 80 mV s^{-1}). It can be observed that all the curves have good rectangular shapes even at a high scan rate of 80 mV s^{-1}, which imply a high rate capability of the MnO_2/a-MCMB composite electrode. This result is different from those of MnO_2/C composites in previous literatures, which suggests that the a-MCMB supported

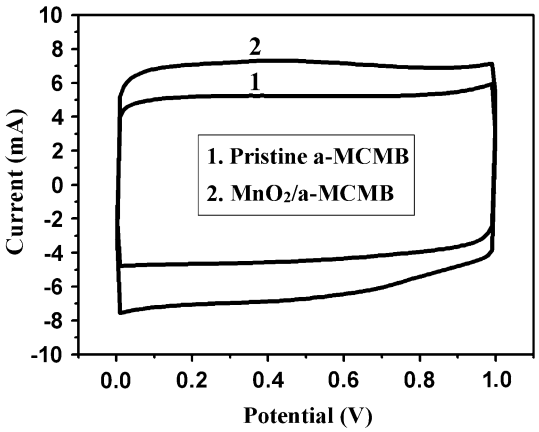

Fig. 6 CV curves of supercapacitor cells based on pristine a-MCMB and MnO_2/a-MCMB composite

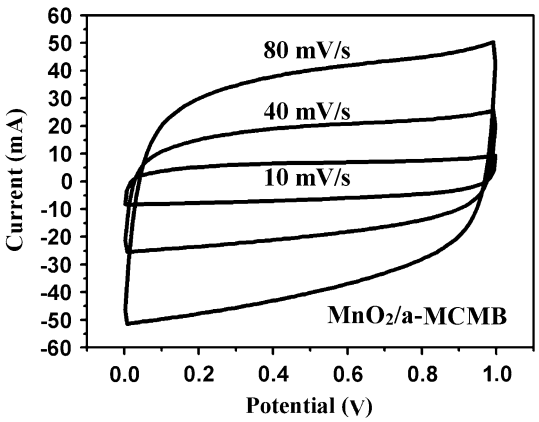

Fig. 7 CV curves of supercapacitor cells based on MnO_2/a-MCMB composite at different scan rates

1-D nano-MnO_2 is of great benefit to the electrolyte penetration and charge transfer owe to the large surface area and good continuity of 1-D nanostructure. Thus these advantages can allow fast kinetics, even at high scan rates, which results in the improvement of the rate capability.

Figure 8 shows the charge/discharge curves of the MnO_2/a-MCMB composite electrode and the pristine a-MCMB electrode in supercapacitor cells at a current density of 135 mA g^{-1}. Both the shapes of the two curves are closely linear and show typical triangle symmetrical distribution at potential region of 0.0–1.0 V, which reveals good capacitive properties of the supercapacitors. The specific capacitance (C_s) of the MnO_2/a-MCMB composite electrode and the pristine a-MCMB electrode were 357 and 296 F g^{-1}, which were calculated from the discharging plots with the following formula:

$$C_T = \frac{I\Delta t}{\Delta V}, \frac{1}{C_T} = \frac{1}{m_1 C_S} + \frac{1}{m_2 C_S} \quad (1)$$

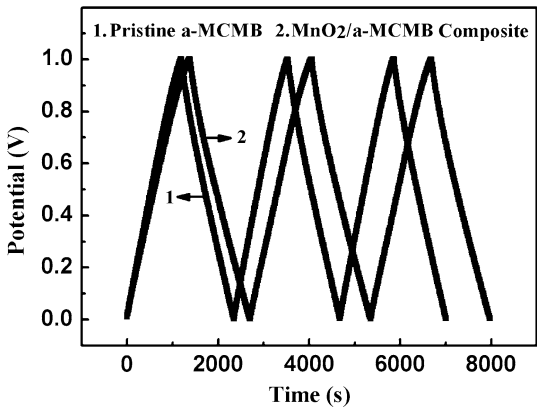

Fig. 8 Galvanostati charge/discharge curves of supercapacitor cells based on pristine a-MCMB and MnO_2/a-MCMB composite

where C_T is total series capacitance of the two electrodes in supercapacitor cell (F), I is the current (A), Δt is the discharging time (s), ΔV is the voltage difference of discharge (V), C_s is the specific capacitance of a single electrode (F g^{-1}), m_1 and m_2 are the active masses of the two electrodes, respectively. Consequently, the C_s based on MnO_2 nanowires in the composite electrode was up to 890 F g^{-1} calculated by deducting the capacitive contribution of a-MCMB from total capacitance of the composite electrode according to formula (2):

$$C_{s-Mn} = \frac{C_{s-Com} - C_{s-C} \times (1-13.08\ \%) \times (1-15.62\ \%)}{15.62\ \%} \quad (2)$$

where $C_{s\text{-}Mn}$ is the C_s based on MnO_2 nanowires; $C_{s\text{-}Com}$ and $C_{s\text{-}C}$ are C_s of the MnO_2/a-MCMB composite electrode and the pristine a-MCMB electrode, respectively.

EIS (see Fig. 9) further gives evidences that the resistance of the MnO_2/a-MCMB electrode is very low which is slightly higher than that of pristine a-MCMB electrode. The equivalent series resistance (ESR) (see the x-intercept) and charge transfer resistance (CTR) (see the semicircles) of MnO_2/a-MCMB electrode is only 0.18 and 0.48 Ω, and the ESR and CTR is 0.18 and 0.33 Ω for the pristine a-MCMB electrode. Such low resistance of MnO_2/a-MCMB electrode is mainly due to the good diffusion of electrolyte ion in the porous material and good contact between the MnO_2 and a-MCMB.

It has been well known that the pseudo-capacitance of MnO_2 is based on the reversible redox process that takes place in the redox transition $Mn^{4+} \leftrightarrow Mn^{3+}$. The generally accepted reactions for the MnO_2 in mild aqueous electrolyte are as follows [23, 24]:

$$MnO_2 + C^+ + e^- \leftrightarrow MnOOC^+ \quad (3)$$

$$(MnO_2)_{surface} + C^+ + e^- \leftrightarrow (MnO_2^- C^+)_{surface} \quad (4)$$

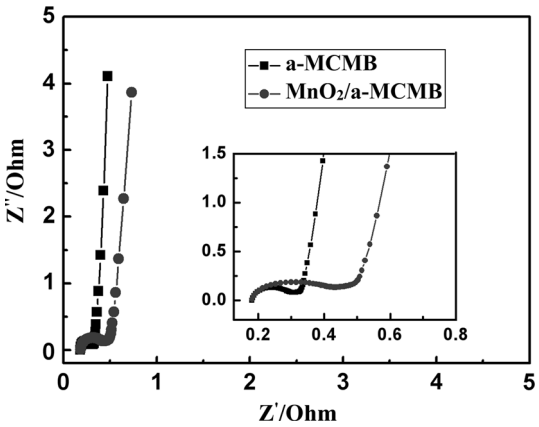

Fig. 9 EIS curves of supercapacitor cells based on a-MCMB and MnO_2/a-MCMB composite

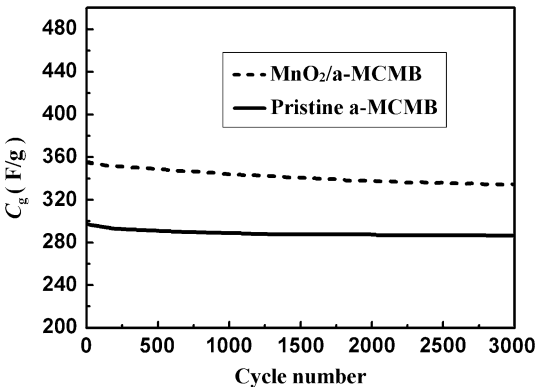

Fig. 10 Cycling stability of of supercapacitor cells based on pristine a-MCMB and MnO_2/a-MCMB composite

where C = Na^+, K^+, or Li^+, and the second mechanism is based on the surface adsorption of electrolyte cations (C^+) on MnO_2.

The 1-D nanostructures of metal oxides have been considered to be more beneficial to higher capacitance than the bulky or particle ones, because these 1-D nanostructures have sufficiently high surface area and high aspect ratio, which will provide a short cation diffusion path length and effective electron-transport continuity and thus result in facile redox reaction and fast charge/discharge for supercapacitor [10, 25]. Moreover, the advantaged crystallographic structure of α-MnO_2 as well as the improvement of electric conductivity of MnO_2 due to the a-MCMB acting as a conductive agent is also constructive to the high capacitance. As a result, the high capacitance of MnO_2 nanowires improved the total capacitance of the MnO_2/a-MCMB composite electrode reasonably.

Since long cycle life is crucial for supercapacitors, the electrochemical stability of the MnO_2/a-MCMB composite electrode and the pristine a-MCMB electrode was examined by charge–discharge cycling at current density of 135 mA g^{-1} and the results are shown in Fig. 10. It is seen from the figure that, after 3,000 cycles, a high C_s of 336 F g^{-1} (with a 93 % capacitance retentivity to the original C_s) could be obtained for the MnO_2/a-MCMB composite electrode while 282 F g^{-1} for the pristine a-MCMB electrode, which indicates a better cycle-stability associated with high capacitance for the MnO_2/a-MCMB composite electrode compared to the pristine a-MCMB electrode.

4 Conclusions

A simple hydrothermal synthesis method for synthesizing α-MnO_2 nanowires with the support of spherical activated carbon a-MCMB was developed in this study. These MnO_2 nanowires with the diameter of less than 50 nm exhibited good network-like distribution on the surface of a-MCMB. Electrochemical measurements showed that the MnO_2/a-MCMB composite electrode is of high specific capacitance, high rate capability and good cycle-stability. The 1-D nanostructure of the MnO_2 grown onto the high surface area a-MCMB demonstrated the good capacitive properties for the supercapacitor application.

Acknowledgments This research was supported by the National Natural Science Foundation of China (21443006), Natural Science Foundation of Guangdong Province (S2013040015162), Guangdong Province and Chinese Academy of Sciences Strategic Cooperative Project (2012B090400003), Science and Technology Project of Maoming (2014006) and Doctor Startup Project of School (513086).

References

1. F. Wang, S. Xiao, Y. Hou, C. Hu, L. Liu, Y. Wu, RSC Adv. **3**, 13059–13084 (2013)
2. K. Jia, X. Zhuang, B. Cheng, S. Shi, Z. Shi, B. Zhang, J. Mater. Sci.: Mater. Electron. **24**, 4769–4773 (2013)
3. L. Yang, M. Li, Y. Zhang, K. Yi, J. Ma, Y. Liu, J. Mater. Sci.: Mater. Electron. **25**, 1047–1052 (2014)
4. C. Lei, N. Amini, F. Markoulidis, P. Wilson, S. Tennisonb, C. Lekakou, J. Mater. Chem. A **1**, 6037–6042 (2013)
5. M. Jeong, K. Zhuo, S. Cherevko, W. Kim, C. Chung, J. Power Sources **244**, 806–811 (2013)
6. Q. Li, X. Sun, K. Lozanob, Y. Mao, RSC Adv. **3**, 24886–24890 (2013)
7. X. Zhang, D. Zhao, Y. Zhao, P. Tang, Y. Shen, C. Xu, H. Lia, Y. Xiao, J. Mater. Chem. A **1**, 3706–3712 (2013)
8. Q. Li, Z. Wang, G. Li, R. Guo, L. Ding, Y. Tong, Nano Lett. **12**, 3803–3807 (2012)
9. X. Lu, M. Yu, G. Wang, T. Zhai, S. Xie, Y. Ling, Y. Tong, Y. Li, Adv. Mater. **25**, 267–272 (2013)
10. Z. Yu, B. Duong, D. Abbitt, J. Thomas, Adv. Mater. **25**, 3302–3306 (2013)
11. L. Chen, J. Kang, Y. Hou, P. Liu, T. Fujita, A. Hirataa, M. Chen, J. Mater. Chem. A **1**, 9202–9207 (2013)
12. X. Lang, A. Hirata, T. Fujita, M. Chen, Nat. Nanotechnol. **6**, 232–236 (2011)

13. Y. Huang, Y. Li, Z. Hu, G. Wei, J. Guo, J. Liu, J. Mater. Chem. A **1**, 9809–9813 (2013)
14. F. Xiao, Y. Xu, J. Mater. Sci.: Mater. Electron. **24**, 1913–1920 (2013)
15. C. Wei, P.S. Lee, Z. Xu, RSC Adv. **4**, 31416–31423 (2014)
16. H. Wang, Z. Li, J. Yang, Q. Li, X. Zhong, J. Power Sources **194**, 1218–1221 (2009)
17. F. Li, W. Chi, Z. Shen, Y. Wu, Y. Liu, H. Liu, Fuel Process. Technol. **91**, 17–24 (2010)
18. C. Wang, H. Hsu, J. Hu, J. Power Sources **249**, 1–8 (2014)
19. T. Brousse, M. Toupin, R. Dugas, L. Athouël, O. Crosnier, D. Bélanger, J. Electrochem. Soc. **153**, A2171–A2180 (2006)
20. S. Devaraj, N. Munichandraiah, J. Phys. Chem. C **112**, 4406–4417 (2008)
21. Y. Li, H. Xie, J. Wang, L. Chen, Mater. Lett. **65**, 403–405 (2011)
22. H. Wang, F. Xiao, L. Yu, B. Liu, X.W. Lou, Small **10**, 3181–3186 (2014)
23. S. Pang, M. Anderson, T. Chapm, J. Electrochem. Soc. **147**, 444–450 (2000)
24. X. Yang, Y. Wang, H. Xiong, Y. Xia, Electrochim. Acta **53**, 752–757 (2007)
25. M. Huang, S. Mao, H. Feick, H. Yan, Y. Wu, H. Kind, E. Weber, R. Russo, P. Yang, Science **292**, 1897–1899 (2001)